PERGAMON

Applied Geochemistry 17 (2002) 301–320

Applied Geochemistry

www.elsevier.com/locate/apgeochem

Rates of sulfate reduction and metal sulfide precipitation in a permeable reactive barrier

S.G. Benner*,[1], D.W. Blowes, C.J. Ptacek, K.U. Mayer[2]

Department of Earth Sciences, University of Waterloo, Waterloo, Ontario, N2L 3G1, Canada

Received 22 May 2000; accepted 31 May 2001
Editorial handling by J.S. Herman

Abstract

A full-scale reactive barrier, utilizing bacterially mediated SO_4 reduction to promote metal sulfide precipitation and alkalinity generation, was installed in August 1995 at the Nickel Rim mine site near Sudbury, Ontario. Monitoring of groundwater chemistry over a 3-a period allows assessment of long-term reactive barrier performance. The overall rate of SO_4 removal within the barrier declined with time by 30% from an initial rate of 58 to 40 mmol l^{-1} a^{-1} 38 months after installation. Over the same time, the rate of Fe removal declined by 50% from 38 to 18 mmol l^{-1} a^{-1}. The degree of SO_4 reduction and Fe sulfide precipitation within the barrier is both spatially and temporally variable. Spatial differences are primarily the result of different residence times due to hydraulic conductivity variations of the treatment material. Temporal variations are likely the result of a decline in organic C availability and reactivity over time and seasonal variations in the rate of SO_4 reduction. Temperatures in the aquifer fluctuate from a low of 2 °C in the winter to a high of 16 °C in the summer and the rate of SO_4 reduction in the summer is nearly twice as great as the winter rate. An effective activation energy (E_a) of 40 kJ mol^{-1} can account for the temperature-induced changes. In Year 3, the barrier removed >1000 mg/l SO_4 and >250 mg/l Fe, demonstrating the long-term viability of this remedial approach. © 2002 Published by Elsevier Science Ltd.

1. Introduction

A full-scale permeable reactive barrier was installed August 1995 in a sand aquifer at the Nickel Rim mine site in Ontario, Canada (Benner et al., 1997) (Fig. 1). The reactive barrier intercepts a groundwater plume, emanating from a tailings impoundment. The groundwater is characterized by elevated concentrations of Fe(II), SO_4 and Ni and and a pH between 5 and 6 (Bain et al., 1999) (Fig. 2). Upon discharge to the surface, the oxidation of Fe(II) and precipitation of Fe (oxy)hydroxides produces acidity and the surface water pH is 2.

The barrier is installed into an alluvium-filled valley and abuts underlying bedrock at the sides and base. The reactive barrier contains organic C in the form of municipal compost which promotes SO_4 reduction and metal sulfide precipitation and increases the alkalinity of the effluent (Benner et al., 1999). The reactive mixture in the barrier is composed of a 1:1 (by volume) mixture of pea gravel and compost (Benner et al., 1997). The compost material consists of partly degraded leafy material and wood chunks of 0.5–3-cm diameter. Sulfate reduction is bacterially mediated and populations of SO_4 reducing bacteria are 5 orders of magnitude higher within the barrier compared to the up-gradient aquifer (Benner et al., 1999; 2000). Iron and SO_4 are primarily removed by precipitation of Fe sulfides and the accumulating mineral phase is mackinawite (FeS) (Herbert et al., 2000). Removal of Fe(II) prevents the generation of acidity when the groundwater discharges to the surface and the addition of alkalinity increases groundwater buffering capacity. This paper presents results of 3a of monitoring, defines rates of SO_4 and Fe removal,

* Corresponding author at current address. Fax: +1-650-725-0979.

E-mail address: sbenner@stanford.edu (S.G. Benner[1]).

[1] Current address: Department of Geologic and Environmental Sciences, Stanford University, Stanford, CA 94305-2115, USA.

[2] Current address: Department of Earth and Ocean Sciences, University of British Columbia, 6339 Stores Road, Vancouver, British Columbia V6T 1Z4, USA.

0883-2927/02/$ - see front matter © 2002 Published by Elsevier Science Ltd.
PII: S0883-2927(01)00084-1

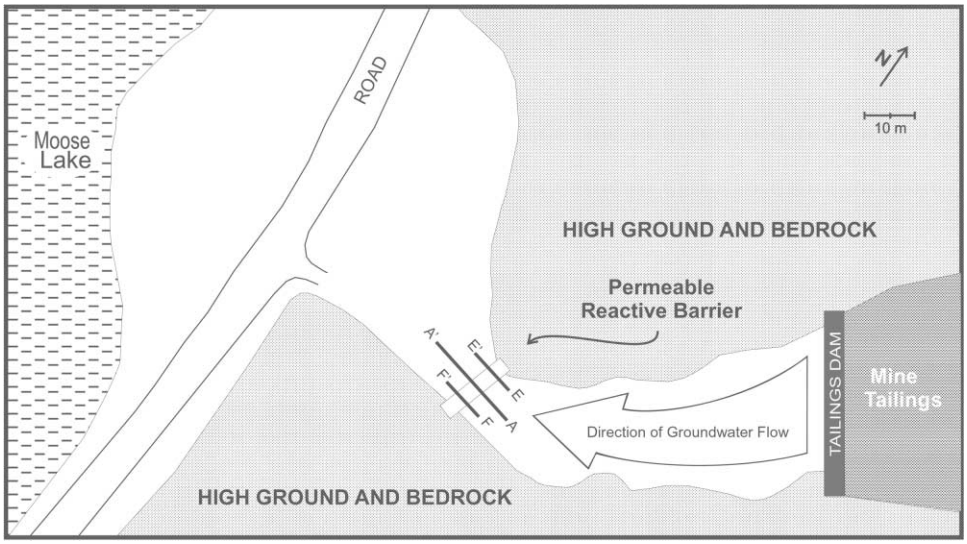

Fig. 1. Map view of Nickel Rim reactive barrier installation showing mine tailings impoundment, groundwater flow path, and locations of reactive barrier and monitoring well transects.

and describes spatial and temporal variations in barrier performance.

2. Methodology

Five centimeter multi-level monitoring wells and 1 cm bundle piezometers were installed along 3 transects parallel to groundwater flow (Figs. 1 and 2). These wells were installed using a gasoline powered vibrating hammer (Dubrovsky, 1986). Samples of groundwater were collected bi-annually from November 1995 to October 1998. Water samples were collected from installed wells using a peristaltic pump and passed through 0.45 μm filters. Samples for cation analyses were acidified to pH < 1 using 12 N trace metal grade HCl. All samples were refrigerated at the field site and stored refrigerated until analyzed at the University of Waterloo or the Falconbridge Ltd. Analytical Laboratories. Concentrations of Al, As, Ca, Fe, K, Mg, Mn, Na, Ni, S, Zn, were determined by inductively coupled plasma emission spectrometry and SO_4, and Cl, by ion chromatography. Determinations of pH (ORION^{TM} Ross 815600 combination electrode or Accumet^{TM} standard 13-620-108 gel filled combination electrode) and Eh (ORION^{TM} 9678BN combination electrode) were made at each piezometer using sealed cells maintained at groundwater temperature. The pH electrode was calibrated using pH 4.0 and 7.0 buffer solutions (traceable to NIST). The performance of the Eh electrode was confirmed using prepared Zobell's solution (Zobell, 1946; Nordstrom et al., 1977) and Light's solution (Light, 1972). Determinations of alkalinity were made in the field by titration with standardized H_2SO_4 using a digital titrator (Hach Instruments Ltd.). Total sulfide was determined in the field colorimetrically using a spectrometer.

The geochemical speciation/mass transfer computer code MINTEQA2 (Allison et al., 1990), adjusted to be consistent with the WATEQ4F database (Ball and Nordstrom, 1991), was used to aid in the interpretation of aqueous geochemical data. Input parameters were Al, Ca, Cl, Fe, K, Mg, Mn, Na, Ni, Si, SO_4, Zn, alkalinity and pH. All dissolved Fe was assumed to be in the Fe(II) oxidation state.

Sediment cores were collected using a 5 cm diameter driven coring device adjacent to well nests RW29, 30, and 31 in September 1997 (Fig. 2). Cores, collected in Al casing, were sealed with plastic caps and refrigerated until analyzed. Sediment was analyzed for most probable numbers (MPN) of SO_4 reducing bacteria and dehydrogenase activity which can be generally correlated with bacterial respiratory activity and used as an index of microbial activity (Ladd, 1978). A detailed description of the bacterial analysis methods can be found in Benner et al. (1999).

The two-dimensional finite element model FLOTRANS (Guiguer et al., 1994) was used to conduct simulations of flow and conservative Cl transport along Transect A–A′ parallel to flow and passing through the reactive barrier. The objective of the modeling was to further quantify and constrain the velocity distribution within the barrier. Modeling was conducted based on the Cl tracer data within the barrier and down-gradient aquifer. High concentrations of soluble Cl contained in the installed compost material provided an *in situ* tracer of groundwater flow through the barrier. Excess compost at the surface also produced elevated Cl concentrations

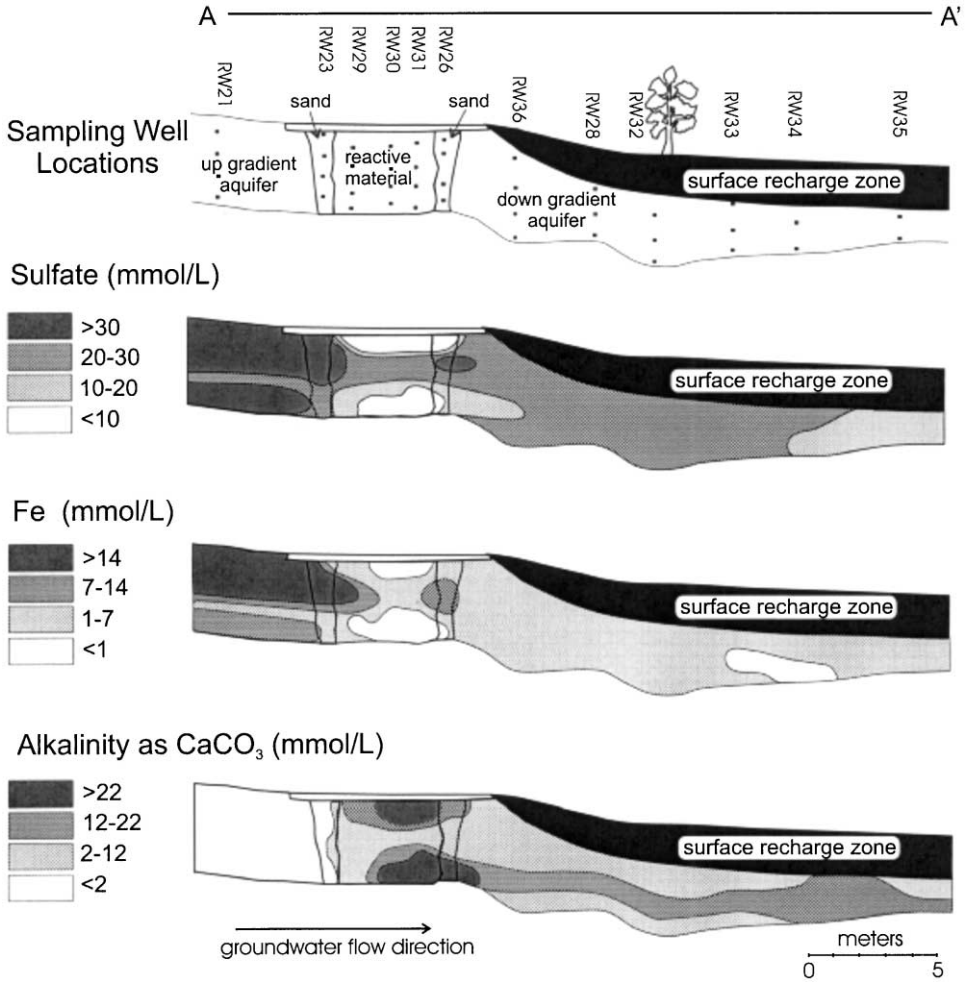

Fig. 2. Cross-sectional profiles through the reactive barrier and Nickel Rim aquifer parallel to groundwater flow along Transect A–A′. Profiles show sampling well locations and dissolved concentrations of SO_4, Fe and alkalinity (as $CaCO_3$) for July 1997. After Benner et al., 1999.

in the surface water, including the water recharging the aquifer on the down-gradient side of the barrier. The modeling was conducted using a uniform grid of 100 by 100 nodes representing a 30 by 3.5 m domain. The left and right boundaries were assigned specified head so that a gradient of 0.016 was established with flow from left to right (Fig. 3). The top of the transect down gradient from the barrier was assigned a specified flux to reflect surface water recharge to the aquifer in this region. A no flow condition was assumed for the remaining boundaries. The initial hydraulic conductivity field was based on previous flow modeling of Bain et al. (1999). Transport boundary and initial conditions were assigned to reflect low background Cl concentrations in the aquifer, high initial Cl concentrations in the barrier, and elevated Cl concentrations in the surface recharge water down gradient of the barrier.

3. Results

3.1. Physical flow

Field-measured water levels indicate that groundwater flow is perpendicular to the barrier installation and generally parallel to Transect A–A′ (Fig. 1). The hydraulic gradient across the barrier (0.016) is slightly lower than the average gradient for the adjacent aquifer (0.02) indicating that the average hydraulic conductivity of the barrier is greater than that of the aquifer. Direct measurement of hydraulic parameters within the barrier has proven difficult. Clogging of well screens by the reactive organic material has prevented development of a good hydraulic connection between monitoring wells and the barrier groundwater. However, the distribution of dissolved Cl concentrations with time yielded information

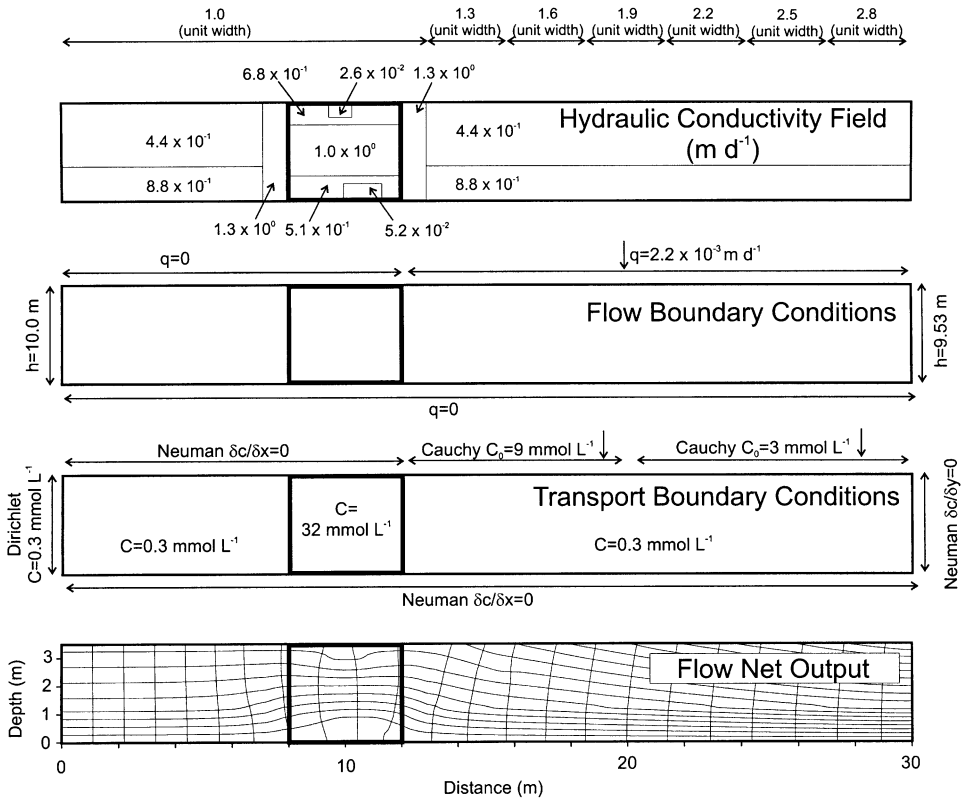

Fig. 3. Flow and transport modeling boundary and initial conditions.

about the nature of groundwater flow through the barrier. The transport of Cl indicates that flow through the barrier is heterogeneous, with higher flow velocities through the central portion of the barrier (Figs. 4 and 5). These tracer data provide a direct measurement of the groundwater velocity through the reactive barrier and indicates a bulk groundwater velocity for the aquifer of approximately 16 m a^{-1}.

The computer transport modeling solution was calibrated based on changes in Cl concentrations with time. Model calibration was achieved by adjustment of the hydraulic conductivity field (Fig. 3). The flow solution is constrained by, and consistent with, the field hydraulic head measurements (Bain et al., 1999), Cl tracer data (Fig. 4), and observed rates of treatment within the barrier (Fig. 6). The flow modeling confirmed an average groundwater velocity for the aquifer of 16 m a^{-1}. With a barrier thickness of 4 m, the average residence time within the barrier is 90 days. The modeling suggests that velocities through the middle of the barrier are approximately 3 times faster (residence time $\approx$60 days) than at the top and base (residence time $\approx$165 days). The flow solution presented should not be considered unique. However, it provides a well-constrained model of the flow field that can assist in determining treatment rates within the barrier.

3.2. Trends in Fe and SO_4 removal

Data collection over the lifetime of the barrier was primarily along Transect A–A′ and data from this transect will be used to assess barrier performance. Along this transect, concentrations of SO_4 and Fe are higher through the central portion of the barrier, while alkalinity values are higher at the top and bottom. These spatial trends are evident in all 7 sampling events over the 3-a of monitoring.

Chemical profiles collected in May and October of 1998 along Transects E–E′ and F–F′ and parallel to Transect A–A′ provide a more complete view of Fe and SO_4 removal in the barrier for that time period (Figs. 7 and 8). Iron and SO_4 concentrations are spatially variable and the trends along each transect are distinct. There is not always a correlation between elevated influent concentrations and elevated concentrations within the barrier, suggesting the degree of removal varies with flow path. Profiles along Transect F–F′ show high input concentrations in the center of the aquifer corresponding to elevated concentrations within the central portion of the barrier. However, along transect E, the highest input concentrations are found at the top of the aquifer while the highest values within the barrier are in the bottom of the profile. Along all transects, trends in SO_4 and Fe

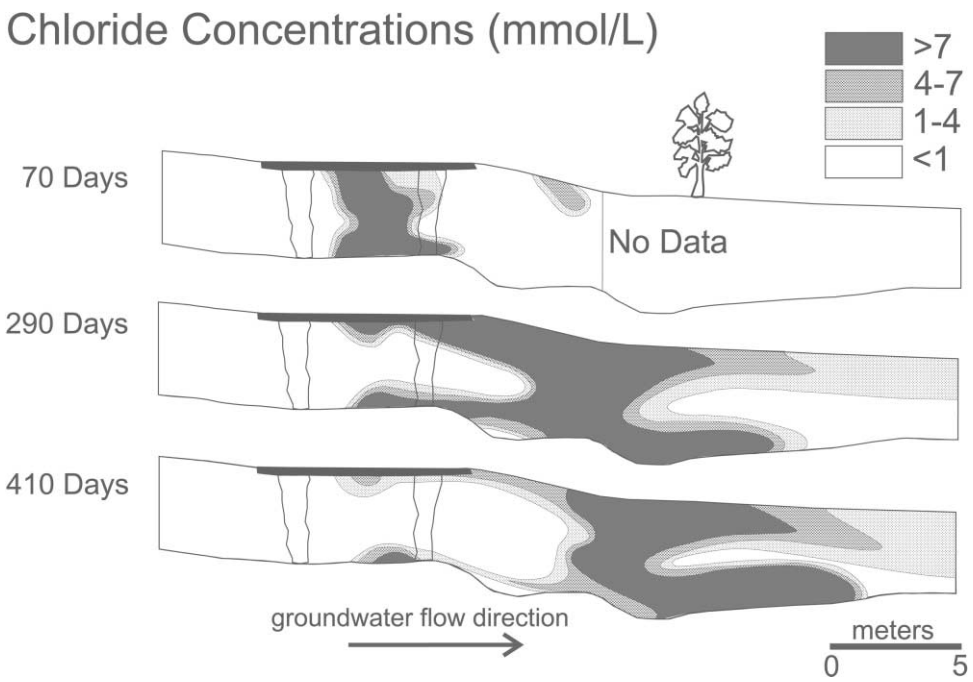

Fig. 4. Field-measured cross-sectional profile of Cl concentrations with time along Transect A–A′.

concentrations are similar; where SO_4 is high, Fe is also elevated and where SO_4 is low, Fe is also low. As along Transect A–A′ (Fig. 2), alkalinity values are elevated where SO_4 and Fe concentrations are low (data not shown).

Vertically averaging concentrations along Transect A–A′ reveal horizontal trends in removal. The horizontal trends in SO_4 and Fe as groundwater passes through the barrier are similar for each of the 7 sampling dates over a 3-a period (Fig. 9). Average input concentrations of SO_4 ranges from 24 to 36 mmol l^{-1} and average output ranges from 12 to 26 mmol l^{-1}. The rate of SO_4 removal based on these vertically averaged values is highest at the front of the barrier. Sulfate concentrations decline by almost 20 mmol l^{-1} between the input well nest (RW23) and the middle well nest (RW30), but exhibit less decline from the middle to the down-gradient well nest (RW31). Vertically averaged influent Fe concentrations range from 7 to 12 mmol l^{-1} with effluent concentrations ranging from <1 to 6 mmol l^{-1}. Like SO_4, the highest rates of Fe removal are at the front of the barrier and there is almost no decline in Fe concentrations from the 2nd to the 3rd well nest within the barrier. Both SO_4 and Fe concentrations in the well nest down gradient of the barrier tend to be elevated compared with those found within the barrier.

3.3. Bacterial distribution

Sulfate reduction is the primary reaction resulting in changes in SO_4, Fe and alkalinity concentrations (Benner et al., 1999). Because this reaction is bacterially mediated, profiles of bacterial populations and bacterial activity provide a measure of reactivity within the barrier. The dehydrogenase assay (DH) can be correlated to overall bacterial respiration, giving an indication of bacterial activity (Ladd, 1978). Fig. 10 shows vertical profiles of SO_4 reducing bacterial populations (SRB) and dehydrogenase activity for sediment cores within the barrier taken adjacent to well nests RW29, 30 and 31. These profiles indicate variations of up to 2 orders of magnitude with depth, showing the heterogeneous nature of bacterial distribution and activity within the barrier. Although the vertical distribution is variable, SRB populations and bacterial activity values tend to be more elevated through the central portion of the barrier, corresponding to the zone of higher SO_4 and Fe concentrations.

3.4. Seasonal variations

There are sufficient spatial and temporal variations in SO_4 and Fe concentrations in the up- and down-gradient waters to obscure seasonal changes in the rate of SO_4 and Fe removal within the barrier. However, a plot of average concentration of constituents within the barrier (12 sampling points), subtracted from the average up-gradient concentration does reveal seasonal cycling (Fig. 11). More SO_4 and Fe is removed and more alkalinity generated in samples collected in the fall compared to spring. These seasonal fluctuations likely reflect

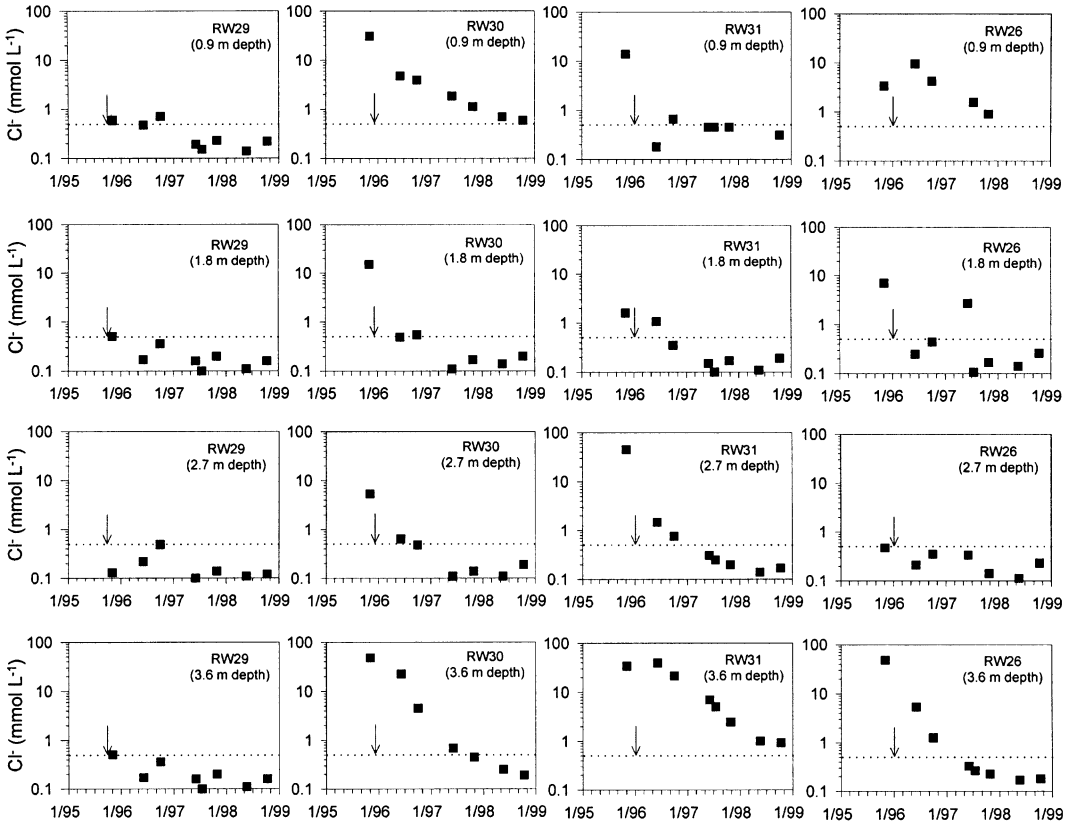

Fig. 5. Chloride concentrations with time for sampling points in well nests RW29, RW30 and RW31 located 0.5, 2 and 3.5 m into the barrier (Fig. 2). Dashed line indicates maximum observed Cl^- concentration of influent water. Arrow marks time at which background would be reached under plug flow conditions and a groundwater velocity of 16 m a^{-1}. Each plot is labeled with the approximate depth below surface.

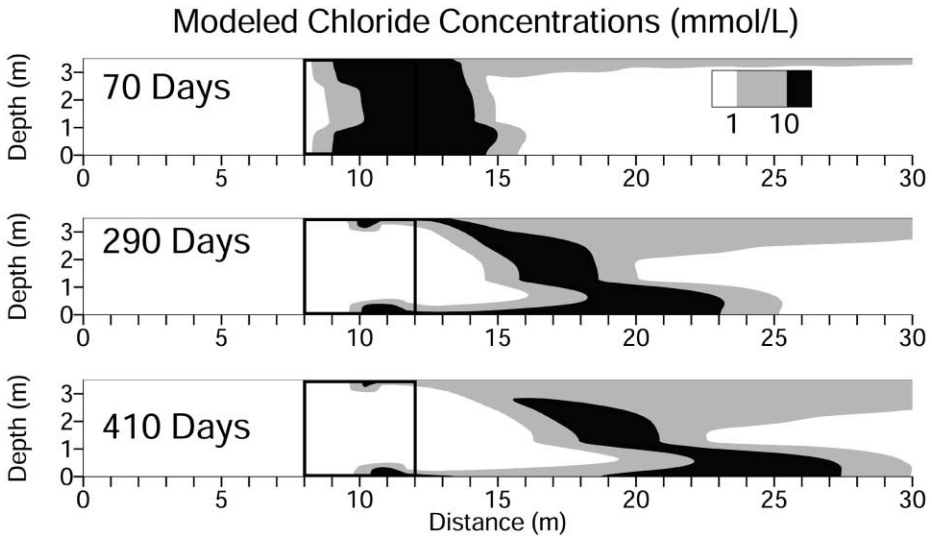

Fig. 6. Modeled cross-sectional profiles of Cl concentrations with time along Transect A–A′.

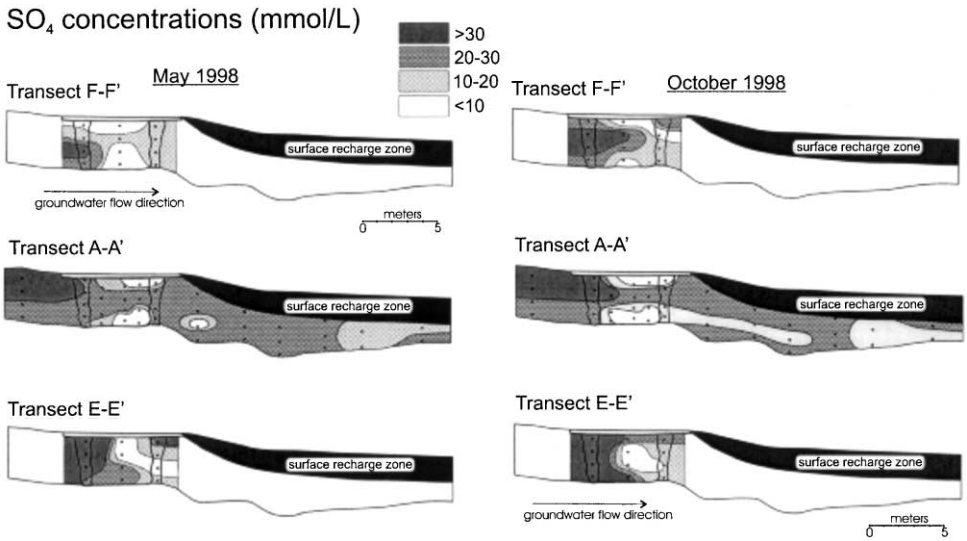

Fig. 7. Cross-sectional profiles of SO_4 concentrations along Transects F, A, and E, parallel to groundwater flow, for the May and October 1998 sampling periods.

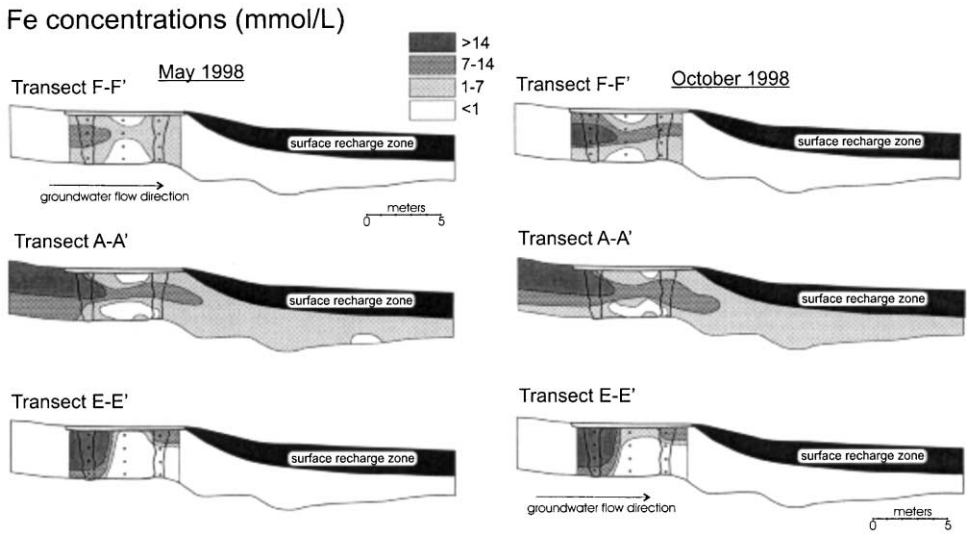

Fig. 8. Cross-sectional profiles along Transects F, A, and E parallel to groundwater flow, of Fe concentrations for the May and October 1998 sampling periods.

changing rates of bacterially mediated SO_4 reduction induced by higher groundwater temperatures during the summer and lower temperatures in the winter.

Groundwater temperatures within the reactive barrier installation exhibit large seasonal variations (Fig. 12). Ground surface temperatures range from $>25\ ^\circ C$ in the summer to $<0\ ^\circ C$ in the winter and the groundwater temperature at 1 m depth varies from 2 to 19 °C. Fluctuations are dampened with depth with seasonal changes at the 3.6 m depth of about 7°. The temperature gradient inverts semi-annually with the highest temperatures at the surface during the summer and the highest temperatures at the base of the barrier during winter. These shifts in groundwater temperature are the product of two factors. First, the water table at the Nickel Rim site is at, or very near, the surface so there is no unsaturated zone to insulate the groundwater from changing air temperatures. Second, surface water infiltrates the aquifer immediately up gradient of the barrier. The temperature of the surface water ranges from $>25\ ^\circ C$ in the summer to 0 °C in the winter.

No measurable difference in groundwater temperature was detected spatially between the up-gradient aquifer and the groundwater within the barrier, indicating the

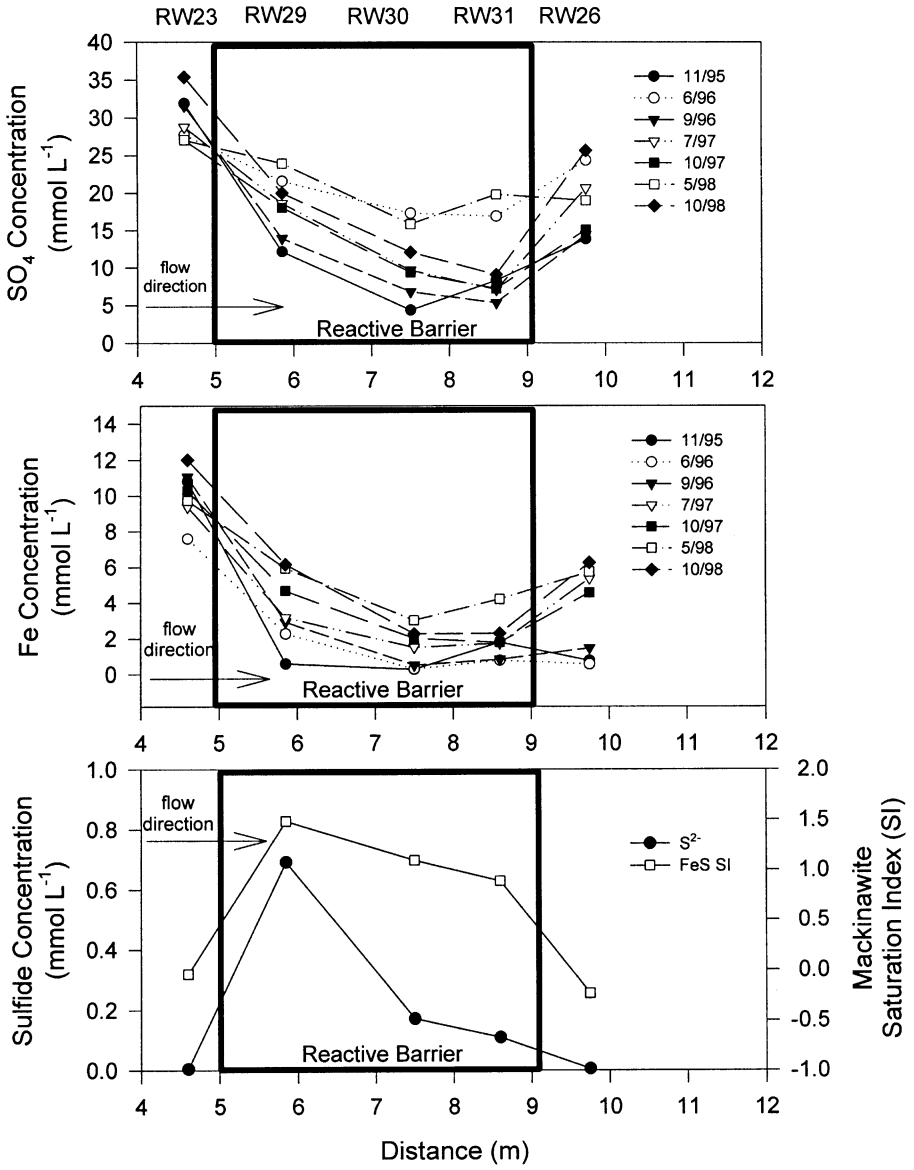

Fig. 9. Vertically averaged trends in concentrations of SO_4, Fe, for all sampling periods, and sulfide concentrations and the saturation index for the mineral phase mackinawite for September 1996.

metabolic processes within the barrier do not affect the groundwater temperature as it passes through the barrier.

4. Discussion

4.1. Heterogeneous flow

A 3-layer model of flow with slower groundwater velocities at the top and bottom of the barrier can explain the bulk Cl distribution. However, the temporal evolution of Cl concentrations for the 12 sampling points within the barrier indicates heterogeneities in groundwater flow rates at a smaller scale (Fig. 5). After 280 days (June 1996 sampling date), Cl concentrations at all sampling points are less than 0.5 of the initial concentration ($\approx$32 mmol l^{-1}), consistent with the residence time within the barrier varying from 60 to 165 days. However, Cl concentrations at many points within the barrier remain elevated after the first bulk pore volume has exited the barrier. Chloride concentrations at some points remain elevated above input concentrations for >1000 days. This residual tailing in Cl concentrations suggests the diffusive release of Cl from aggregates of

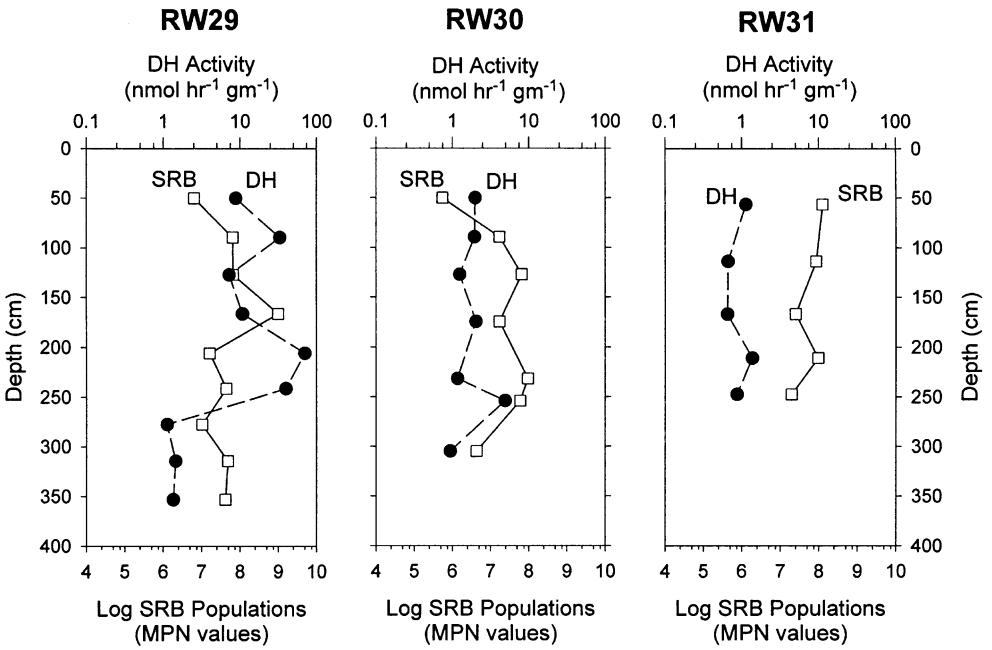

Fig. 10. Vertical profiles of populations of SO_4 reducing bacteria (SRB) and overall bacterial activity as measured by dehydrogenase activity (DH) for cores taken adjacent to well nests RW29, RW30, and RW31.

low K material (Gillham et al., 1984). Small variations in the gravel to compost ratio in the reactive mixture can produce a large hydraulic conductivity contrast. A change of 5% in the fraction of gravel (from 40 to 45%) can produce an order of magnitude change in hydraulic conductivity (Benner et al., 1997). The presence of Cl tailing indicates that there is slow moving pore water within the barrier which has a residence time markedly longer then that estimated from the bulk Cl plume and associated flow modeling.

4.2. Elevated concentrations down gradient

The horizontal profiles indicate Fe and SO_4 concentrations are often elevated in sampling wells down gradient compared to those within the barrier (Fig. 9). Groundwater bypassing treatment by flowing around the barrier could explain this trend. However, flow bypassing the barrier through underlying or adjacent crystalline bedrock is unlikely for the following reasons. The hydraulic gradient across the barrier is lower than the adjacent aquifer, indicating that there is no hydraulic force driving water around the barrier. Elevated Fe and SO_4 concentrations on the down gradient side of the barrier are observed in sampling wells in the middle of the profile, and are not limited to the sides or base where bypassed water would re-enter the down-gradient aquifer. Finally, concentrations of SO_4, Fe and alkalinity in down-gradient well nests always reflect some degree of treatment; if a large fraction of untreated water was bypassing the barrier, some wells would likely exhibit concentrations reflective of no treatment.

An alternative explanation for higher Fe and SO_4 values on the down-gradient side of the barrier is heterogeneous flow coupled with sampling that is biased towards a volume average. Because slower moving water in the barrier has undergone a greater degree of SO_4 reduction, this water will tend to have lower concentrations of SO_4 and Fe, and higher alkalinity compared to adjacent, faster moving water. At the scale of the observed 3 layer vertical stratification in the barrier, there is a positive correlation between zones of low hydraulic conductivity (K) and lower concentrations of SO_4 and Fe and higher alkalinity values. Observed Cl tailing (Fig. 5) indicates that spatial variation in flow velocities also occurs on a smaller scale within the barrier. Although the contribution of water from these smaller-scale, low K, zones to the flux through the barrier may be small, the contribution to the volume within the barrier may be significant. Within this conceptual model of flow through the barrier, volume-average sampling would result in lower concentrations of SO_4 and Fe and higher alkalinity compared to flux-averaged sampling (Parker and van Genuchten, 1984). In the down-gradient, non-reactive zone, no correlation between hydraulic conductivity and water chemistry exists and volume-biased sampling will not result in a systematic shift in water chemistry. Assuming volume biased sampling occurs, the profile in the down-gradient well nest is likely a better estimate of average mass fluxes through the barrier.

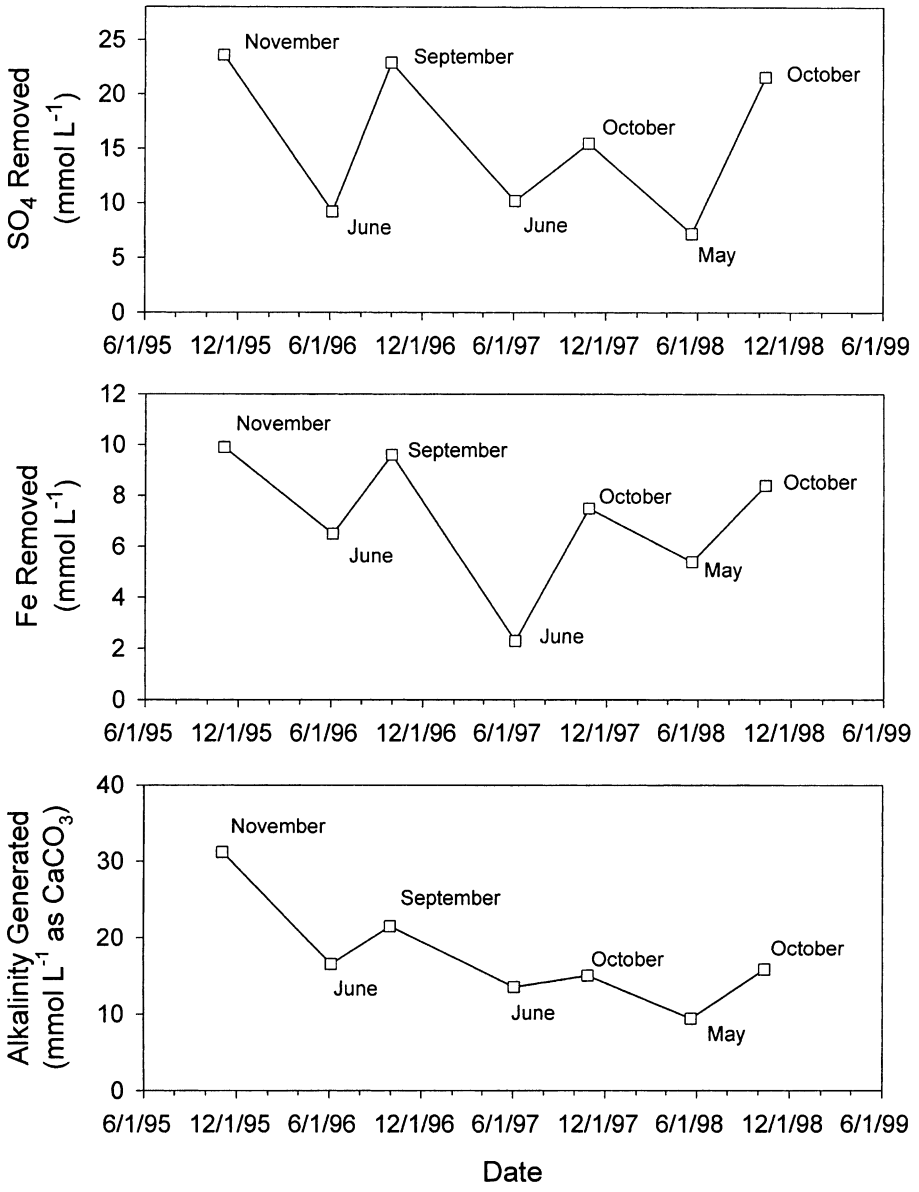

Fig. 11. Average concentrations of SO_4 and Fe removed and alkalinity added with time. Based on the RW23 concentrations- concentrations of all points ($n=12$) within the barrier.

4.3. Reactivity or residence time

Flow data suggest that higher rates of removal of SO_4 and Fe observed along cross section A–A′ at the top and bottom of the barrier are the product of variation in residence time. However, these trends may also be caused by variations in reactivity. If the observed vertical trends of higher SO_4 and Fe removal at the top and bottom of the profile were the result of variations in reactivity, bacterial populations and bacterial activity would be higher in these zones. This trend is not observed (Fig. 10). In fact, the higher values for both SRB populations and DH are generally found in the central portion of the barrier where the distribution of Cl indicates the water is moving more rapidly and SO_4 and Fe concentrations are highest. These limited data suggest that the bacterial populations may be responding to, and not controlling, observed vertical variations in water chemistry. Although spatial variations in reactivity cannot be discounted, the available data suggests

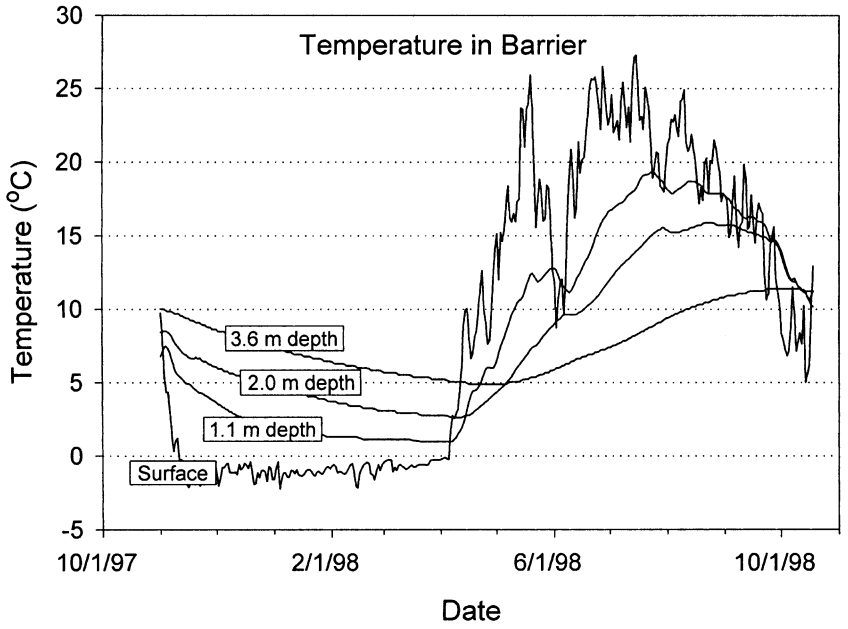

Fig. 12. Measured temperature data within the barrier over a one year period. Curves are shown for ground surface temperature, 1.1, 2.0, 3.6 m depths.

that the observed differences in Fe and SO_4 concentrations with depth in the barrier are primarily the product of variations in residence time.

4.4. Bulk treatment rate

An overall rate of SO_4 and Fe removal for the barrier was calculated based on the change in concentrations between up- and down-gradient well nests along Transect A–A′. Fig. 13 shows the vertically averaged molar concentrations of SO_4 and Fe for well nests up (RW23) and down gradient (RW26) of the barrier with time. Although there are large variations over the 3-a of monitoring, profiles of water entering the barrier indicate that average SO_4 concentrations are $\approx$27 mmol l^{-1} and Fe concentrations are $\approx$10 mmol l^{-1}. Profiles of down-gradient concentrations with time show SO_4 concentrations increasing from <17 mmol l^{-1} to >23 mmol l^{-1} and Fe concentrations increasing from <1 to about 6 mmol l^{-1}.

The differences between up- and down-gradient concentrations (RW23 and RW26) are plotted versus time in Fig. 13c. A linear fit was applied to the collected data because the limited data did not suggest a more complex model. However, the decline in rate may not be linear over the longer term. The change in constituent concentrations can be expressed as a change in concentration (mmol l^{-1}; left-hand axis) or as a removal rate (mmol l^{-1} a^{-1}; right-hand axis). The removal rate is calculated as:

$$\text{Concentration removed} = (\text{rate})t_R \quad (1)$$

where the concentration removed (mmol l^{-1}) is equal to the influent minus the effluent, t_R is the residence time in years, and the rate is expressed in mmol l^{-1} a^{-1}. In this calculation, an average t_R of 90 days is assumed. The bulk removal rate for SO_4 is initially 58 mmol l^{-1} a^{-1} and declines to 40 mmol l^{-1} a^{-1} while the Fe removal rate is initially 38 mmol l^{-1} a^{-1} and declines to 18 mmol l^{-1} a^{-1}. The calculated bulk rates for SO_4 and Fe removal for the barrier represent an average of the rates along different flow paths and are a function of barrier thickness.

By subtracting effluent from influent concentrations along each transect in Figs. 7 and 8 it is possible to calculate an average 3-dimensional removal rate for the barrier in 1998. The average removal for all points for the May and October data is 17 mmol l^{-1} SO_4 and 9 mmol l^{-1} Fe. The vertically averaged amount removed along the centerline transect (Transect A–A′) for that same time period is 12 mmol l^{-1} SO_4, and 6 mmol l^{-1} Fe. This comparison indicates that, although Transect A–A′ is generally representative of changes through the barrier, this transect may underestimate, by about 1/3, overall SO_4 and Fe removal. These bulk removal rates mask both spatial and seasonal variability in treatment within the barrier and assume that the rate is zero order with respect to SO_4 concentrations. However, the rate of SO_4 reduction is a function of SO_4 concentration and the rate of SO_4 reduction is also influenced by temperature (Boudreau and Westrich 1984, Jorgensen, 1977). Since both SO_4 concentrations and groundwater temperature vary within the barrier, a more complex expression of SO_4 reduction within the barrier is warranted.

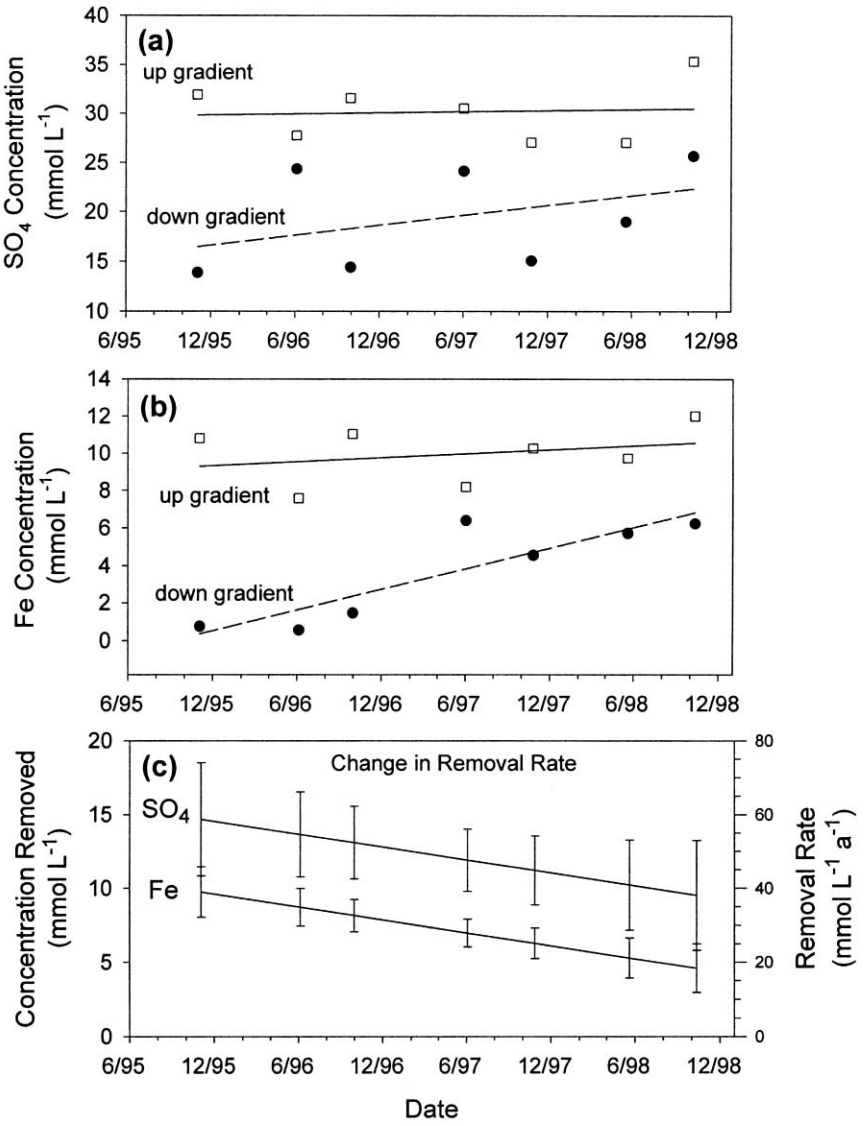

Fig. 13. (a) Vertically averaged concentrations of SO_4 in the well nests RW23 (up gradient) and RW26 (down gradient) versus time. (b) Vertically averaged concentrations of Fe in the well nests RW23 (up gradient) and RW26 (down gradient) versus time. (c) Removal of SO_4 and Fe based on the difference between RW23 and RW26 (up gradient- down gradient) concentrations versus time. Error bars reflect one standard error.

4.5. Calculating a rate constant

The rate of bacterially mediated sulfate reduction, as measured in marine sediments, can be expressed by the hyperbolic rate equation:

$$\text{sulfate removed} = t_R\left[k\left(\frac{[SO_4]}{K_s + [SO_4]}\right)\right] \quad (2)$$

where SO_4 is in mmol l^{-1}, t_R is the residence time in years, k is the effective rate constant and the half saturation constant (K_s) equals 1.62 mmol l^{-1} (Boudreau and Westrich 1984; Roychoudhury et al., 1998). This rate formulation is empirically used to express the behavior of a reaction limited by availability of a reactant. When SO_4 concentrations are much greater than the saturation constant, the fractional term approaches unity, the rate is zero order and SO_4 concentrations will decline linearly. As the SO_4 concentration nears the saturation value, the fractional term becomes smaller, and the rate approaches 1st order dependence on SO_4 concentration. The rate of SO_4 reduction decreases and asymptotically approaches zero as the SO_4 concentration approaches zero. With a K_s of 1.62 mmol l^{-1}, the rate of SO_4

reduction at a SO_4 concentration of 5 mmol l^{-1} will be 75% of the zero order rate at higher SO_4 concentrations.

Within the Nickel Rim barrier, the rate of SO_4 removal declines as SO_4 concentration declines (Fig. 9). This trend is observed despite the vertically averaged SO_4 concentrations within and down gradient of the reactive barrier being generally much greater than 5 mmol l^{-1}. The heterogeneous nature of flow through the barrier can reconcile this apparent contradiction. Assuming that variations in reactivity do not have a major impact on the rate of SO_4 reduction, the rate of SO_4 removal is expected to remain nearly constant while SO_4 concentrations remain above about 5 mmol l^{-1}. If the rate of flow were uniform through the barrier, then the profile of SO_4 concentration would be expected to decline linearly across the barrier until concentrations approached 5 mmol l^{-1}, at which point the rate of removal would decline. However, flow rates (and residence times) vary in the barrier with flow path (Fig. 14). The SO_4 concentrations along the slower flow path at the base of the barrier exhibit a generally linear decline in concentration until the middle well nest where concentrations drop below the 5 mmol l^{-1} level. The SO_4 profile shows little decline from that point to the down-gradient side of the barrier. Along the faster, central section of the barrier, SO_4 concentrations decline less steeply. Sulfate concentrations do not fall below the 5 mmol l^{-1} value, there is no obvious break in slope, and concentrations decline over the entire profile. These more discrete flow paths produce curves that more closely follow the Boudreau and Westrich (1984) hyperbolic rate equation. At the front of the barrier, the SO_4 concentration along all flow paths is above 5 mmol l^{-1} (Fig. 14). Sampling indicates that with distance into the barrier the fraction of pore water with a SO_4 concentration below 5 mmol L^{-1} increases. The result of this trend is that the overall bulk rate of SO_4 reduction decreases with distance into the barrier, even though the vertically averaged effluent SO_4 concentration is above 5 mmol l^{-1} (Fig. 9). Limited sulfide data show elevated concentrations at the first well nest, which is consistent with the observed higher rates of SO_4 reduction at the front of the barrier (Fig. 9).

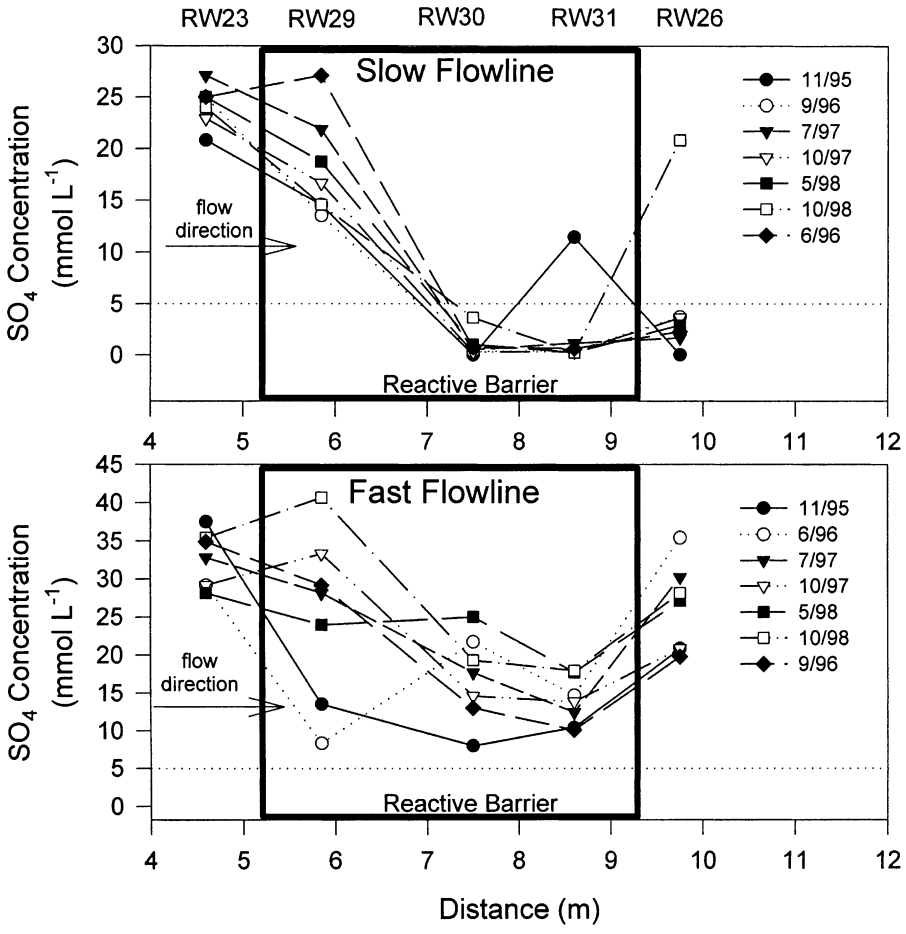

Fig. 14. Trends in concentrations of SO_4 along slow flow path at bottom of the barrier and fast flow path in the middle of the barrier.

The distribution of flow path residence times through the barrier may be complex. However, a simplified model based on bimodal flow can explain the observed SO_4 profiles within the barrier. Fig. 15 shows the 3-a average field values along the fast and slow flow paths. Predicted profiles for fast and slow flow paths are calculated using the rate equation after Boudreau and Westrich (1984). Along the fast flow path through the center of the barrier and slow flow path at the base of the barrier, the residence time and amount of SO_4 removed is known. Assuming that K_s equals 1.62 mmol l^{-1}, it is possible to solve for the effective rate constant (k). Data from up and down gradient of the barrier are used to constrain curves for the fast and slow flow paths (Fig. 15). The calculated rate constant (k) equals 47 mmol l^{-1} a^{-1} for an average groundwater temperature of 9 °C. This effective rate constant is assumed to be a function of groundwater temperature and the amount and reactivity of the organic C. It may also reflect other, unidentified factors influencing the rate of SO_4 reduction.

Using the calculated effective rate constant (k), and adjusting the residence time, curves matching SO_4 concentrations within the barrier indicate a residence time on the order of 370 days. These calculated residence times are consistent with zones of very slow moving water within the barrier as suggested by the Cl tailing and apparent chemical bias in volume averaged samples.

The effective rate constant ($k = 47$ mmol l^{-1} a^{-1}) is very similar to the bulk rate calculated from the average influent and effluent values (49 mmol l^{-1} a^{-1}). It is anticipated that because of heterogeneous flow, the bulk rate would be lower than the calculated rate constant. That these rates are essentially the same illustrates how flux through the barrier is dominated by water passing along the faster flow paths. Along the faster flow paths, SO_4 concentrations remain high, the fractional term in the hyperbolic rate equation reduces to unity, and the resulting rate expression approximates the previously calculated 0th order bulk rate of SO_4 removal. Only for water associated with the very slow flow paths (e.g. 370 day residence times) do low SO_4 concentrations impact the rate of removal.

4.6. Fe removal rates

The rate of Fe removal is also greater at the front of the barrier (Fig. 16). Profiles of Fe along both fast and slow flow paths show Fe concentrations declining more steeply at the front of the barrier. This trend follows SO_4, suggesting Fe removal is closely related to SO_4 reduction. If the rate of Fe sulfide precipitation were more rapid than SO_4 reduction, than one would expect SO_4 concentrations and the saturation index for the precipitating SO_4 mineral phase (mackinawite–FeS) to remain uniform across the barrier. However, elevated sulfide concentrations and higher saturation indices for mackinawite are observed at the front of the barrier, suggesting that the rate of Fe sulfide precipitation may be limiting (Fig. 9). The laboratory-determined rate of FeS precipitation of Rickard (1995) is between 10^2 and 10^6 times greater than the observed rate of SO_4 reduction in the barrier. Therefore, limitations on the rate of FeS precipitation may be the product of transport and not precipitation processes. Within the barrier, there is generally excess SO_4 after consumption of the Fe (compare Figs. 14 and 16). Within zones of slower flow, most

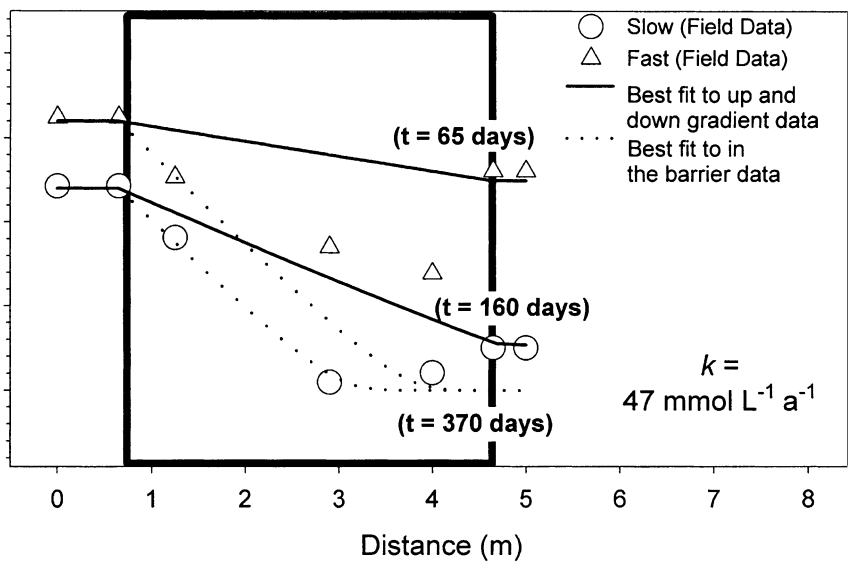

Fig. 15. Trends along fast and slow, and all flow paths averaged for all sampling periods and modeled rates of SO_4 removal based on hyperbolic formulation.

of the Fe is removed and sulfide concentrations become elevated. It is likely that the effective rate of Fe removal is at least partially limited by transport of dissolved sulfide from these slow zones to adjacent zones of faster flow where Fe concentrations are higher. Dissolved sulfide concentrations (and mackinawite SI values) decline by an order of magnitude by the first well nest in the down-gradient aquifer. These observations suggest that the effective rate of Fe sulfide precipitation may be slower than that of SO_4 reduction within the barrier, but is probably limited by the generation and transport of dissolved sulfide. Therefore, the rate of Fe removal by FeS precipitation in the barrier is ultimately limited by the rate of SO_4 reduction.

4.7. Quantifying temperature effects

The Arrhenius equation relates the effect of changing temperature on the rate of reaction. The Arrhenius equation can be expressed as:

$$\log\frac{k_1}{k_2} = \frac{E_a}{2.303R}\left[\frac{1}{T_2} - \frac{1}{T_1}\right] \quad (3)$$

where k_1 is the rate coefficient at temperature T_1 (Kelvin), k_2 is the rate coefficient at temperature T_2 (Kelvin), R (8.314×10^{-3} kJ mol^{-1} K^{-1}) is the gas constant and E_a (kJ mol^{-1}) is the activation energy of the reaction. Before applying this equation to the rate of SO_4 reduction in the reactive barrier, the activation energy (E_a) must be defined. The sulfate reduction reaction sequence is complex and it is likely that the rate of SO_4 reduction is limited by the supply of low molecular weight compounds produced by fermentative activity (Westrich and Berner, 1984; Boudreau and Ruddick, 1991). In this application of the Arrhenius equation, E_a does not specifically refer to the activation energy of the SO_4 reduction reaction but is defined as an apparent activation energy and is simply a measure of the response of the overall rate of SO_4 reduction to a change in temperature.

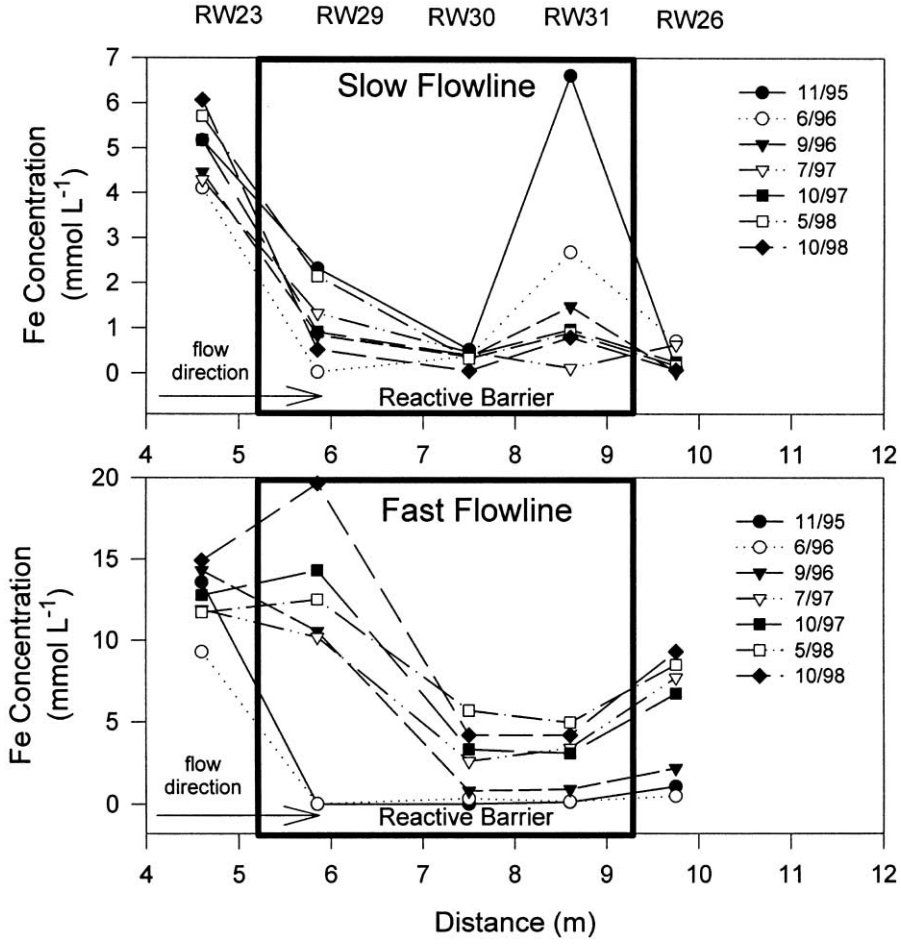

Fig. 16. Trends in concentrations of Fe along the slow flow path at the bottom of the barrier and the fast flow path in the middle of the barrier.

Letting k_2 equal the rate coefficient of SO_4 reduction as expressed by the zero order function from Fig. 13;

$$k_2 = -0.0049(t) + b \quad (4)$$

where t is the date in number of days, b is the y-intercept, T_2 equals the average annual temperature at 2 m depth (9 °C), while T_1 is equal to the sinusoidal temperature function expressing the 2-m depth field-measured temperature data (Fig. 12):

$$T_1 = 8.9843 - 5.8[\sin(2(\pi)(t)/365 - 150.55)] \quad (5)$$

where t is the date expressed as number of days. Therefore, the unknowns are the y-intercept (b) and the apparent activation energy (E_a). A solution is obtained by simultaneously solving for the y-intercept and E_a to achieve a best fit to the field-collected SO_4 concentration data (k_1) (Fig. 17). The resulting effective E_a is 40 kJ mol^{-1}.

Specifying a range of E_a values and solving for the best fit to the field data suggests the range of effective E_a that provide a reasonable fit (values shown as dashed lines in Fig. 17). These plots indicate that the field data constrain the minimum E_a value, but do not constrain the maximum E_a value. However, the lowest observed SO_4 concentration (maximum removal value) provides an upper limit on the E_a. Concentrations in well nest RW31 during the fall sampling event reflect water that passed through the barrier during the period of highest SO_4 reduction rates (the month of August). The lowest vertically averaged concentration measured for SO_4 for RW31 is 5 mmol l^{-1}. This value, subtracted from the input concentration, can be used to constrain the maximum SO_4 reduction rate in the barrier (stepped horizontal line, Fig. 17). With this constraint on the highest rate of SO_4 reduction, the range of potential E_a is limited to a value very close to the best-fit 40 kJ mol^{-1} value. The modeled curve describes the observed field data quite well indicating that the observed seasonal variations in SO_4 removal can be attributed to the effect of changing temperature on the rate of SO_4 reduction.

Previous workers have determined changes in SO_4 reduction rate with temperature and calculated a range of apparent E_a from 21 to 134 kJ mol^{-1} (Jorgensen, 1977; Westrich and Berner, 1988; Sagemann et al., 1998, and references therein). Westrich and Berner (1988) also determined that the effective E_a increases with the age of the organic matter, presumably because newer organic C is more easily oxidizable. These previous studies were conducted on ocean sediment organic matter that is generally older (and probably less labile) than that used in the reactive barrier. The calculated E_a for the Nickel Rim barrier is at the lower end of the range of values determined in previous studies confirming that the organic material used in the barrier is labile and reactive.

Because SO_4 reduction is the rate-limiting step in Fe removal, the rate of sulfide precipitation may approach thermodynamic equilibrium. Changing temperature can also potentially influence Fe concentrations by changing the solubility of the precipitating Fe sulfide. The potential effect that changing temperature has on the solubility

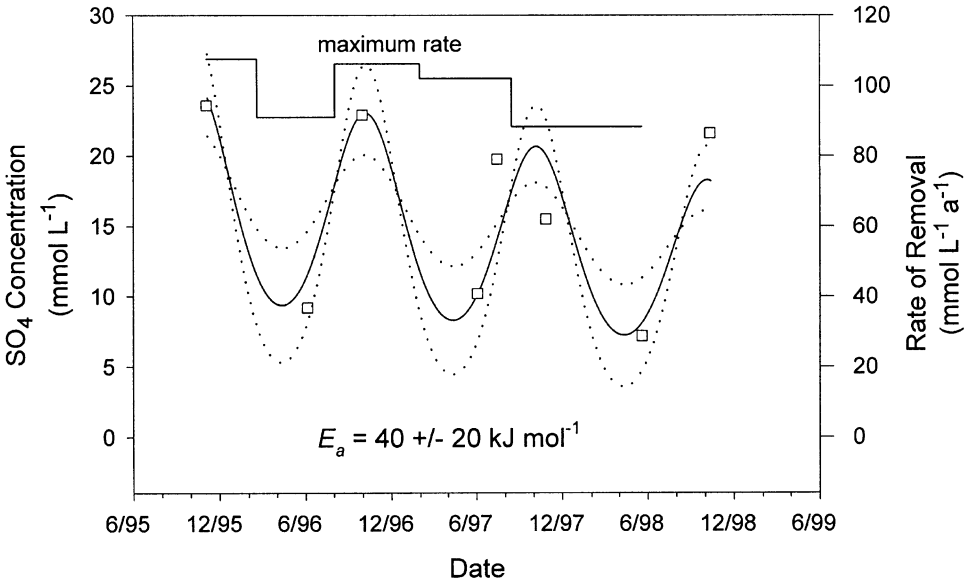

Fig. 17. The curve based on Arrhenius equation (solid line) for observed temperature induced fluctuations in SO_4 removal (square boxes) yielding an apparent activation energy $E_a = 40$ kJ mol^{-1}. Dashed curve shows sensitivity of fit to changing E_a by ±20 kJ mol^{-1}. Stepped solid line indicates maximum rate based on observed removal in well nest RW23 (down gradient).

product of the precipitating mineral phase mackinawite can be estimated using the van't Hoff equation:

$$\log K_2 = \log K_1 + \frac{\Delta H_R}{2.303R}\left[\frac{1}{T_1} - \frac{1}{T_2}\right] \quad (6)$$

where K_1 is the equilibrium constant at temperature T_1, K_2 is the equilibrium constant at T_2 and ΔH_R is the enthalpy of reaction and is assumed to be constant with changing temperature. A similar approach to that used to calculate the affect of temperature on reaction rate can be taken. If the precipitation reaction is written as:

$$Fe^{2+} + HS^- \Longleftrightarrow FeS_{(s)} + H^+ \quad K = 10^{3.75} \quad (7)$$

K_1 equals $K_{mackinawite}$ (Benning et al., 2000) at $T_1 = 25$ °C, T_2 is defined by the 2 m depth temperature function and the enthalpy (ΔH_r) for mackinawite precipitation is specified as -52.1 kJ mol^{-1}(Benning et al., 2000). The equation can be solved for the remaining unknown, K_2. Assuming equilibrium conditions and that Fe and HS^- vary equally, the theoretical change in Fe concentration can be calculated (Fig. 18). This sinusoidal plot is inverse to the observed changes in Fe and SO_4, suggesting that the changes in Fe concentration cannot be attributed to seasonal variation in mackinawite solubility.

The changing solubility of the potentially important secondary precipitating phases siderite ($FeCO_3$) and gypsum ($CaSO_4{\cdot}2H_2O$) may also contribute to the observed seasonal changes in dissolved SO_4 and Fe. The enthalpy of reaction (ΔH_R) for siderite precipitation is 22.2 kJ mol^{-1} (Allison et al., 1990) indicating that siderite is less soluble at higher temperatures. Therefore, the changing solubility of siderite may also contribute to the seasonal variation in Fe concentrations. The enthalpy of reaction (ΔH_R) for gypsum is near zero (0.46 kJ mol^{-1}) and the annual 17 °C change within the barrier will have little effect on gypsum solubility or associated SO_4 concentrations. It should be noted that the solubilities of siderite and gypsum are also directly dependent on CO_3^{2-} and Ca^{2+} activities, respectively, and the seasonal changes in the solubilities of both of these minerals are difficult to predict with simple calculations.

4.8. Other sinks for SO_4 and Fe

The relative rates of SO_4 and Fe removal and accumulation (based on solid phase extraction data, Herbert et al., 2000) indicate that the removal of Fe and SO_4 in the Nickel Rim barrier is not limited to precipitation of sulfide mineral phases (Tables 1 and 2). The solid phase extraction data does indicate that sulfides are the dominant sink for S and Fe in the reactive barrier. However, in portions of the barrier, the precipitation of siderite ($FeCO_3$) and gypsum ($CaSO_4$) and the formation of organic sulfide compounds may also contribute to the Fe and S accumulating in the solid phase (Benner et al., 1999; Herbert et al., 2000). Rates based on solid phase accumulation and aqueous phase removal for Fe and S show good agreement given the uncertainties associated with these calculations (compare Tables 1 and 2). A notable exception is the accumulation rate for S along the slow flow path. The aqueous removal rate is over 3 times greater than the solid phase accumulation rate. It is possible that degassing of H_2S can account for the observed excess SO_4 removed. Degassing is observed above the barrier, however, this gas has not been analyzed and it is unclear if this mechanism can account for a significant loss of S. Calculated rates of H_2S degassing from an artificial wetland treating acid mine drainage by SO_4 reduction were orders of magnitude smaller than sulfide precipitation as a sink for SO_4 (Machemer et al., 1993).

The ratios of S:Fe removal and accumulation also vary with flow path. Along the fast flow path the S:Fe removal ratio is 0.65:1 and the accumulation ratio is

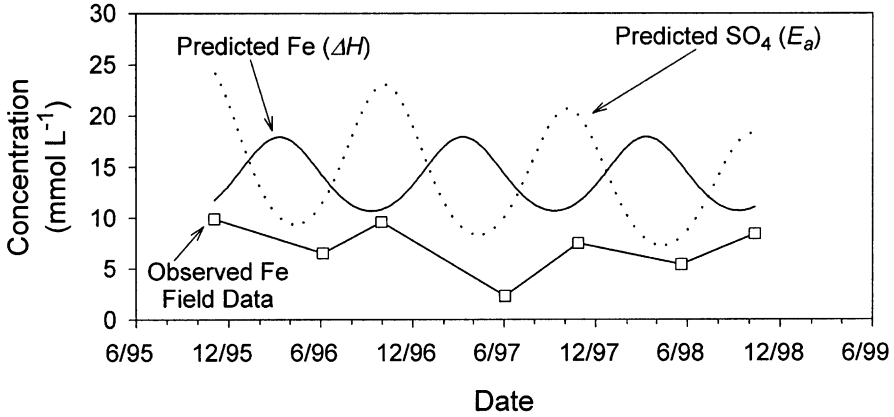

Fig. 18. Observed (square boxes) and predicted Fe concentrations with time based on: (1) changing solubility of mackinawite (based on van't Hoff equation, ΔH) and (2) changing rates of H_2S generation expressed as SO_4 removal (based on Arrhenius equation, E_a).

Table 1
Rates of S and Fe removal based on changes in aqueous concentrations (influent–effluent) and estimated residence times[cd]

Flow path	SO_4 removed [a,b] (mmol l^{-1} pv^{-1})	Fe removed [a,b] (mmol l^{-1} pv^{-1})	Residence time (days)	SO_4 removal rate (mmol l^{-1} a^{-1})	Fe removal rate (mmol l^{-1} a^{-1})	S:Fe removal ratio
Ave.	13	8	90[c]	53	32	1.7:1
Slow	31	12	370[d]	31	12	2.6:1
Fast	5	7.7	80[d]	23	36	0.65:1

[a] Range in values based on (influent–effluent) sampling 3 months to 23 months after installation.
[b] pv equals pore volume.
[c] Assuming groundwater velocity of 16 m a^{-1}.
[d] Based on estimated maximum (18 m a^{-1}) and minimum (3.9 m a^{-1}) velocities for barrier.

Table 2
Rates of S and Fe removal based on solid phase digestions (from Herbert et al., 2000)

S removal rate (mmol l^{-1} a^{-1})[a]				
Flow path	Sulfides[b]	Sulfate[c]	Organic	Degassing
Slow	21	<1	4	?
Fast	30	6	<1	?
Fe removal rate (mmol l^{-1} a^{-1})[a]				
Flow path	Sulfides[d]	Non-sulfides[e]	Other?	
Slow	18	<1	?	
Fast	28	14	?	
Totals (mmol l^{-1} a^{-1})[a]				
Flow path	Total S	Total Fe	S:Fe ratio	
Slow	25	18	1.4:1	
Fast	36	42	0.85:1	

[a] From Herbert et al. (2000), based on average accumulation from 3 months to 23 months after installation. The following ratios were used for rate conversion: barrier material composed of 40% gravel, 20% compost, and 40% water.
[b] Equals operationally defined acid volatile S (AVS) + total reduced S (TRS).
[c] Value is total inorganic SO_4 estimated pore water SO_4.
[d] Sulfide Fe based on sulfide S assuming 1:1, S:Fe ratio for AVS, 2:1 for pyrite and no S as elemental S.
[e] Total Fe- sulfide Fe.

0.85:1. Removal by precipitation of mackinawite (FeS) would result in a S:Fe removal and accumulation ratio of 1:1. These measured S:Fe ratios suggest an additional solid phase sink for Fe exists. Solid phase extraction data indicates that 30% of the accumulated Fe is present in a non-sulfide phase (Herbert et al., 2000). Saturation index values indicate near equilibrium with respect to siderite. It is possible that precipitation of this mineral phase is occurring along the fast flow path. Along the slower flow path, the S:Fe removal ratio is 2.6:1 and the accumulation ratio is 1.4:1. The differences between these two ratios can be attributed to the accumulation of S in the organic fraction of the solid phase (Herbert et al., 2000) and, possibly, degassing of H_2S.

These accumulating solid phases produce little change in porosity. At the maximum accumulation rate of 36 mmol l^{-1} a^{-1} the volume fraction of sulfides (assuming a bulk density of 4 g cm^{-3}) accumulated within the barrier after 3 a is on the order of 1%. This change in porosity is unlikely to produce measurable changes in flow through the barrier.

4.9. Long term trends

Solid phase rate data with time indicate a rapid decline in the rate of SO_4 reduction during the first 3 months and a more gradual decline from 3 to 23 months after installation (Herbert et al., 2000). Although this trend is only based on accumulation rates over 3 sampling periods, it is consistent with a model of organic matter composed of fractions of varying reactivity where the most reactive material is consumed first and overall reactivity asymptotically approaches zero (Westrich and Berner, 1984; Boudreau and Ruddick, 1991). The timing of aqueous sampling sessions did not record the initial high rate and the data plotted in Fig. 13 likely represent the later time period of the curve where reactivity declined more gradually. Extending the trend in SO_4 reduction into the future is speculative, but within the generally accepted models of organic C reactivity (Westrich and Berner, 1984; Boudreau and Ruddick, 1991 and references therein), the rate of SO_4 reduction is predicted to decrease more gradually with time.

4.10. Implications for performance and design

Assuming the average input concentrations of SO_4 (30 mmol l^{-1}) and Fe (10 mmol l^{-1}) and a 1:1 removal ratio, the minimum residence time for removal of >95% of the Fe in the Nickel Rim barrier is approximately 90 days. Despite an average residence time approximately equal to the minimum required residence time of 90 days, complete removal of Fe is not achieved. Less Fe is removed than predicted because the low flow

zones are underutilized for Fe removal; along these slower flow lines all Fe is removed and excess sulfide generated is not utilized for mackinawite precipitation. In addition, when the SO_4 concentration drops near the half saturation constant (K_s), the rate of SO_4 reduction will decline.

Specific enhancements to the reactive mixture composition to improve homogeneity and barrier performance may include increasing the gravel fraction, selecting a different particle size distribution for the organic mixture, or choosing a more reactive organic C material. The costs of any enhancements to barrier design must be weighed against simply installing a thicker barrier or replacing the barrier more often.

At the Nickel Rim site, the average air temperature is only a few degrees lower than at the bottom of the aquifer. Therefore, application of an insulating layer above the aquifer will produce a more uniform SO_4 reduction rate but will result in only a small increase in the annually averaged rate of SO_4 reduction. At sites where the average groundwater temperature is significantly greater than the average air temperature, insulating the aquifer may boost barrier performance. Conversely, when the average air temperature is greater than the average groundwater temperature, insulating the aquifer may decrease performance. Increasing barrier thickness will also decrease the impact of seasonal temperature fluctuations; designing a barrier with a residence time of >1 year would eliminate temperature-induced fluctuations in concentrations of the effluent waters.

The inclusion of temperature dependence in the rate equation allows comparison to previous laboratory column studies of Waybrant (1995). In this laboratory study, flow-through columns containing organic C were used to simulate a reactive barrier for SO_4 reduction and metal sulfide precipitation. The input water for the laboratory column was chosen to match the groundwater in the Nickel Rim aquifer and the organic mixture used in the barrier was based on the mixtures used in the column studies. In this laboratory study, conducted over a 2-a period at 25 °C, the SO_4 reduction rate was 280 mmol l^{-1} a^{-1}. Normalizing this rate to the average temperature in the Nickel Rim aquifer (9 °C) results in a rate of 103 mmol l^{-1} a^{-1}, approximately twice the rate observed in the aqueous phase field data. The difference in rate may be, at least in part, due to differences in organic C content. The organic content of the column studies was approximately twice as great as in the Nickel Rim barrier. The similarity of the rates indicates that the laboratory column experiments were a good predictor of the treatment rate in the field installation.

5. Conclusions

In this study, a reactive barrier for acid mine drainage effluent was assessed. The rate of SO_4 reduction and metal sulfide precipitation declined by 30 and 50%, respectively, over 3 a. Despite this decline, in its third year of operation, the barrier removed >1000 mg l^{-1} SO_4 and >250 mg l^{-1} Fe from the groundwater. These results indicate that reactive barriers can provide long-term treatment of groundwater containing elevated concentrations of SO_4 and Fe. This work has illustrated the potential importance of preferential flow and fluctuating temperature in reactive barrier performance and has provided an approach for quantifying these influences. Relatively small variations in hydraulic conductivity can result in potentially significant differences in residence time. In barriers that are reaction rate limited, these differences in residence time will result in decreased barrier performance. When the treatment reaction is bacterially mediated, accounting for changing groundwater temperature is critical to predicting contaminant removal rates. This study indicates that the 'rule of thumb' of twice the reaction rate for each increase of 10 °C provides a good estimate of the effect of temperature on SO_4 reduction. Reactive barrier designs must account for these spatial and temporal variables and barriers should be constructed to treat the contaminants along the fastest flow path under the lowest anticipated treatment rate.

Acknowledgements

This research was made possible by generous support from the Natural Science and Engineering Research Council of Canada and Falconbridge Ltd. The authors would also like to thank the reviewers Thomas Wildeman and Carl Moses as well as the Associate editor Janet Herman, their comments greatly improved the final manuscript.

References

Allison, J.D., Brown, D.S., Nova-Gradac, K.J., 1990. MINTEQA2/PRODEFA2, A geochemical assessment model for environmental systems: version 3.0 user's manual. Athens, GA, U.S. E.P.A.

Bain, J.G., Blowes, D.W., Robertson, W.D., 1999. Hydrogeochemistry of a sand aquifer affected by drainage from the Nickel Rim tailings. J. Contam. Hydrol 41, 23–47.

Ball, J.W., Nordstrom, D.K., 1991. User's Manual for WATEQ4F, with Revised Thermodynamic Data Base. U.S.G.S., Open File Report 91–183.

Benner, S.G., Blowes, D.W., Gould, W.D., Herbert Jr, R.B., Ptacek, C.J., 1999. Geochemistry of a permeable reactive barrier for metals and acid mine drainage. Environ. Sci. Technol. 33, 2793–2799.

Benner, S.G., Blowes, D.W., Ptacek, C.J., 1997. Full-scale porous reactive wall for the prevention of acid mine drainage. Ground Water Monit. Remed. 17, 99–107.

Benner, S.G., Gould, W.D., Blowes, D.W., 2000. Microbial populations associated with the generation and treatment of acid mine drainage. Chem. Geol. 169, 435–448.

Benning, L.G., Wilkin, R.T., Barnes, H.L., 2000. Reaction pathways on the Fe-S system below 100 degrees C. Chem. Geol. 167, 25–51.

Boudreau, B.P., Ruddick, B.R., 1991. On a continuum representation of organic matter diagenesis. Am. J. Sci. 291, 507–538.

Boudreau, B.P., Westrich, J.T., 1984. The dependence of bacterial sulfate reduction on sulfate concentration in marine sediments. Geochim. Cosmochim. Acta 48, 2502–2516.

Dubrovsky, N.M., 1996. Geochemical Evolution of Inactive Pyritic Tailings in the Elliot Lake Uranium District. PhD thesis, Univ. Waterloo, Waterloo, ON, Canada.

Gillham, R.W., Sudicky, E.A., Cherry, J.A., Frind, E.O., 1984. An advection-diffusion concept for solute transport in heterogeneous unconsolidated geologic deposits. Water. Resour. Res. 20, 369–378.

Guiguer, N., Molson, J., Franz, T., Frind, E., 1994. FLOTRANS User Guide Ver. 3.0: Two-Dimensional Steady-State Flownet and Advective-Dispersive Contaminant Transport Model. Waterloo Hydrogeologic Inc. Waterloo, Ontario, Canada.

Herbert Jr, R.B., Benner, S.G., Blowes, D.W., 2000. Solid phase iron- sulfur geochemistry of a reactive barrier for treatment of mine drainage. Appl. Geochem. 15, 1331–1343.

Jorgensen, B.B., 1977. The sulfur cycle of a coastal sediment (Limfjorden, Denmark). Limnol. Oceanog 22, 814–832.

Ladd, J.N. 1978. Origin and range of enzymes in soil. In: Burns, R.G. (Eds), Soil Enzymes. Academic Press, pp. 51–96.

Light, T.S. 1972. Standard solution for redox measurements. Anal Chem. 44, 1038–1039.

Machemer, S.D., Reynolds, J.S., Laudon, L.S., Wildeman, T.R., 1993. Balance of S in a constructed wetland built to treat acid mine drainage, Idaho Springs, Colorado. USA. Appl. Geochem. 8, 587–603.

Nordstrom, D.K., Jenne, E..A, Ball, J.W., 1977. Thermochemical redox eqilibria of Zobells solution. In: Everett, A.J., Ball, J.W. (Eds), Chemical Modeling of Natural Systems. pp. 51–79.

Parker, J.C., van Genuchten, M.T., 1984. Flux-averaged and volume-averaged concentrations in continuum approaches to solute transport. Water Resour. Res. 20, 866–872.

Rickard, D., 1995. Kinetics of FeS precipitation: part 1. Competing reaction mechanisms. Geochim. Cosmochim. Acta 59, 4367–4379.

Roychoudhury, A.N., Viollier, E., Van Cappellen, P., 1998. A plug flow-through reactor for studying biogeochemical reactions in undisturbed aquatic sediments. Appl. Geochem. 13, 269–280.

Sagemann, J., Jorgensen, B.B., Greeff, O., 1998. Temperature dependence and rates of sulfate reduction in cold sediments of Svalbard, Arctic Ocean. Geomicrobiol. J. 15, 85–100.

Waybrant, K.R. 1995. The Prevention of Acid Mine Drainage Using In Situ Porous Reactive Walls: A Laboratory Study. MSc thesis, Univ. Waterloo, Waterloo, Ontario, Canada.

Westrich, J.T., Berner, R.A., 1988. The effect of temperature on rates of sulfate reduction in marine sediments. Geomicrobiol. J. 6, 99–117.

Westrich, J.T., Berner, R.A., 1984. The role of sedimentary organic matter in bacterial sulfate reduction: the *G* model tested. Limnol. Oceanogr. 29, 236–249.

Zobell, C.E., 1946. Studies of redox potential of marine sediments. Bule. Am. Assoc. Petrol. Geol 30, 477–513.